The International Journal of Advanced Manufacturing Technology (2021) 117:3465–3475
https://doi.org/10.1007/s00170-021-07786-w

ORIGINAL ARTICLE

Effect of heat treatment on microstructure and mechanical characteristics of 316L stainless steel parts fabricated by hybrid additive and subtractive process

Shuoshuo Qu[1,2] · Yadong Gong[3]

Received: 4 November 2020 / Accepted: 24 July 2021 / Published online: 30 August 2021

Abstract
The effect of solution heat treatment on the mechanical and microstructural properties of 316L stainless steel parts fabricated through hybrid additive and subtractive process (HASP) is explored. These techniques synergistically combine additive manufacturing directed energy deposition (DED) with subtractive manufacturing (SM) technique in a single machine, and they provide an important opportunity to improve material utilization, part complexity and quality management in functional components. Thin-wall specimens were manufactured by HASP to investigate the effect of the solution heat treatment at different temperatures and different holding times on the microstructure and the resultant mechanical properties, such as the Vickers micro-hardness and tensile property. The results show that the content of δ and σ phases can be optimized via heat treatment. While the solution treatment temperature and time increase, the content of the σ and δ phases in the γ matrix can distinctly decrease, which causes the strength to degrade but the ductility to increase. These results suggest that the microstructure and the resulting mechanical properties of HASP-fabricated samples can be adjusted through the adjustment of solution heat treatment.

Keywords Solution heat treatment · Microstructure · Vickers micro-hardness · Tensile property · Hybrid additive and subtractive process

Nomenclature

HASP	Hybrid additive/subtractive process
DED	Directed energy deposition
AM	Additive manufacturing
SM	Subtractive manufacturing
HAZ	Heat affected zone
SEM	Scanning electron microscopy
LSCM	Laser scanning confocal microscope
FCC	Face centred cubic
BCC	Body centred cubic
WQ	Water quenching
UTS	Ultimate tensile strength
YS	Yield strength
ETF	Elongation to failure
P	Laser power
V	scan speed
h	Layer thickness
v_Z	Milling linear speed
a_e	Amount of radial feed
a_p	Amount of axis feed
f_z	Feed per tooth

✉ Yadong Gong
gongyd@mail.neu.edu.cn

Shuoshuo Qu
qushuoshuo@sdu.edu.cn

[1] Center for Advanced Jet Engineering Technologies (CaJET), School of Mechanical Engineering, Shandong University, Jinan, Shandong 250061, People's Republic of China

[2] Key Laboratory of High Efficiency and Clean Mechanical Manufacture, Shandong University, Ministry of Education, Jinan, Shandong 250061, People's Republic of China

[3] School of Mechanical Engineering and Automation, Northeastern University, Shenyang 110819, People's Republic of China

1 Introduction

316L stainless steel (SS) is extensively applied in high-temperature bolts, marine, biomedical applications and other industries with a stable austenitic microstructure because of its

strong corrosion resistance, good high-temperature strength, resistance to inter-granular corrosion, machinability and other characteristics [1, 2]. In the twenty-first century, innovation is essential to ensure competitive advantages and maintain the sustainable development of the company in the era of the knowledge economy and information age. Additive manufacturing (AM) technique is a prevalent and important representative of a manufacturing process that has matured rapidly in the past few decades and has been gradually applied to all walks of life: aerospace, automotive, medical, military, mould manufacture and so on as an advanced material processing skill. Contrary to the traditional subtractive manufacturing (SM) technology, which is a "top-down" material removal machining process, AM is a "bottom-up" process that adds material to three-dimensional components from a feedstock via line by line and then layer upon layer forming and consolidation. A wide range of complex shapes and higher utilization ratios of the material are produced via a computer-controlled laser beam source [3–5]. AM methods including directed energy deposition (DED) [3], laser melting deposition (LMD) [4] and direct metal deposition (DMD) [5] have been made. Common to all of these processes is that metals, whether it is powder or wire, are directly melted using a laser beam or electric arc [6]. Moreover, the "staircase effect" is one of the most important and basic characteristic of all of the abovementioned, which gives rise to the layer-wise approximation of component geometries, residual stresses and the partial bonding of small particles, which lead to the problem of surface quality degradation [7]. Furthermore, the temperature gradient and geometric shape of the molten pool have a significant effect on the processes of metal additive manufacturing. Temperature gradients and correlated surface tension could draw attention to quick flow dynamic motions, leading to the "dishing" or "humping" during the solidification process [8]. Long thin molten pools can cause spheroidization, thus decreasing the surface quality, uniformity of the material property and part density [9]. Mechanical subtractive processes, such as milling, drilling and grinding, have been widely applied to additive manufacturing processes, and they can obtain better precision and surface quality characteristics as well as residual stresses are released. As a result, the hybrid additive and subtractive process (HASP), which combine additive and subtractive processes in a single machine, have drawn a great deal of attention owing to their ability to exploit the advantages of each single process while minimizing their shortcomings [10, 11]. The combination of additive and subtractive technologies has been put forward and developed to fabricate the finished components, also including the reuse and remanufacture of high-valve parts. Zhu et al. [10] used the hybrid manufacturing (HM) method to fabricate any type of component with a complicated structure and studied the influence of the process parameters on the part distortions that occurred in the AM process. The results indicate that the length, height, and layer thickness of the part have remarkable impact on the deformations of the parts. Liu et al. [11] put forward a topology optimization method to obtain parts with geometrical complexity and dimensional accuracy by hybrid additive-subtractive manufacturing, which has been successfully implemented by designing a few 3D structures. The method is being extended to adopt an unstructured grid of high quality at present, and its formulation and capability will be reported in the future.

However, the unique conditions generate some specific problems, such as the precipitated intergranular phases that are rich in Cr in the heat affected zone (HAZ) and hot cracking that exists in the DED process under the context of HASP owing to the rapid solidification and then quick cooling [12]. At high temperatures, austenite is the equilibrium phase; nevertheless, the equilibrium phases include delta-ferrite (δ), sigma (σ) and carbides such as M23C6 under ambient temperature on the basis of the Fe-Cr-Ni pseudo-binary diagram [13]. It has also been shown that the amount of δ-ferrite in austenitic stainless steel can improve cracking susceptibility and decrease segregation; moreover, it is generally believed that the δ-phase can be used as a strengthener for high strength, and it is widely used in welded and cast steel as well [14]. However, the hard and brittle sigma phase with a tetragonal crystal structure appears in austenitic stainless steel if the temperature is kept at 400 to 900 °C, which can decrease the mechanical properties, such as fracture toughness and ductility [15]. Prior studies have shown that the σ phase and carbides would have an adverse effect on the performance of stainless steel [16]. Therefore, to acquire the required mechanical property, it is essential to change the microscopic structure in the 316L SS components within the HASP. In general, heat treatment is one of the commonly used processes to soften stainless steel, eliminate unnecessary phases and residual stress in stainless steel and improve microstructure and mechanical properties [17]. The heat treatment temperature is between 950 and 1150 °C, and then water quenching (WQ) can be conducted to effectively make the carbides and σ phase dissolve in the steel [18]. The heat treatment temperature and time ought to be carefully designed for fear of dispensable gain growth [19]. To the authors' knowledge, not so much has been described systematically on the microstructure and mechanical properties of HASP-fabricated 316L samples when subjected to heat treatment.

In the present work, the AISI 316L SS powder as a starting material was employed to fabricate metal components. The influence of solution heat treatment at different temperatures and different holding times on the microstructural feature, including the phase transformation behaviours and mechanical properties, such as tensile properties and Vickers micro-hardness of 316L SS parts, was detailed discussed. The study may provide the theoretical foundation for the HASP to increase efficiency, reduce costs and lead times

and reliably fabricate 316L SS components with optimized microstructure and mechanical properties.

2 Material and experimental methods

2.1 Material

In this work, gas atomization AISI 316L SS powder with spherical shape and diameters ranging from 10 to 130 μm was chosen as the starting material. A scanning electron microscopy (SEM) image of AISI 316L SS powder and the corresponding particle size distribution are shown in Fig. 1. The detailed chemical composition (wt. %) of the 316L SS powder is listed in Table 1. The powder has a great deal of small particles that may interfere with fluidity owing to high inter-particle friction. However, to a great extent, the fine particles can increase the specific superficial area of the composite, resulting in high energy absorptivity of the laser beam [20]. The powder was dried at a temperature of 373 K in drying furnaces for the elimination of the moisture and oxygen remaining in the powder in the DED forming process, which also occurs under the context of HASP [20].

2.2 Hybrid additive and subtractive process

The experimental study was produced by the five-axis HASP machine (SVW80C-3D), which is shown in Fig. 2a. The machine has two processing programs: the laser head of additive manufacturing directed energy deposition (DED), as shown in Fig. 2b, and surface finishing technology by a CNC milling head, as shown in Fig. 2c. In the HASP, laser deposition is utilized to deposit layer by layer. A great deal of material waste, which is commonly seen in the traditional SM process, is avoided in the AM process. Furthermore, the powder can be successfully reused without significantly losing its property. However, during the DED process, the surface of the deposited layer is uneven with a thin oxide scale and stair steps, which have a cumulative effect on the requirement of precision for the part in the Z-axis direction [21]. To overcome this shortcoming, when a layer is deposited, the top surface is processed by CNC milling to achieve a smooth surface of determinate thickness for further deposition. This procedure is repeated until the required component is completed. At last, the inner and outer surface contours are processed by milling process to eliminate the stair steps on the surface and obtain a fine surface state of the metal part. Fig. 2 d and e show examples of the CNC milling process and additive deposition process, respectively.

Table 1 Chemical compositions (wt. %) of the 316L SS powders

Component	C	Si	Mn	Cr	Ni	Mo	Fe	S/P
wt. %	0.02	0.5	1.2	17.0	13.0	2.5	Bal.	<0.01

In order to study solution heat treatment on the mechanical and microstructural properties of 316L cube-shaped samples (length of 140 mm, width of 2 mm and height of 40 mm) manufactured by HASP, according to the previous experimental experience, the parameters of the DED process were as follows: the powder feed rate was 1 g/min, the laser power (P) was 1000 W, the scan speed (V) was 360 mm/min and the layer thickness (h) was set at 0.5 mm. Subsequently, for the sake of surface quality improvement of the DED process, dry milling technology as an SM process was carried out for the finishing machining of the component. The dry milling processing parameters mainly include the following: the feed per tooth (f_z) was set to 0.25 mm, the milling linear speed (v_Z) was 120 m/min, the amount of axis feed (a_p) was 0.5 mm, and the amount of radial feed (a_e) was set to 0.2 mm. The scanning strategy was rotating by 90° to the previous layer. The detailed processing parameters of the hybrid additive and subtractive process were described in our previous work [22, 23]. The substrate of 40# steel with dimensions of 160 mm × 160 mm × 20 mm was set and levelled on the building platform. Prior to the fabrication process, the plate was milled successively to remove an extremely thin oxide layer on the surface of the work piece. The process and schematic of HASP-manufactured stainless steels with dimensions of 140 mm × 2 mm × 40 mm are shown in Fig. 3 a and b, respectively.

2.3 Characterization of microstructures and mechanical properties

After HASP, the specimens with dimensions of 5 mm × 5 mm × 5 mm were cut from the substrate by wire electrical discharge machining to microstructural analysis. The microstructure of the HASP before and after applying solution heat treatment to the 316L samples was investigated by a laser scanning confocal microscope (LSCM). A schematic of the microstructure analysis specimens taken from areas is illustrated in Fig. 3b. The metallographic samples along the building direction of as-deposited specimens, known as the cross section of HASP-manufactured components, underwent cutting, grounding and polishing with classical experimental procedures, and the freshly polished sections were etched with a solution (4 g CuSO4, 20 ml HCl and 20 ml distilled water) prior to microstructure characterization.

The room temperature tensile tests of the 316L samples before and after the solution treatment were conducted on a WDW-100E electronic universal material testing machine (made by Panasonic, Japan) with a maximum load of 100 kN and cross-head separation rate of 5 mm/s. The tensile test samples with the specified dimensions were cut by wire

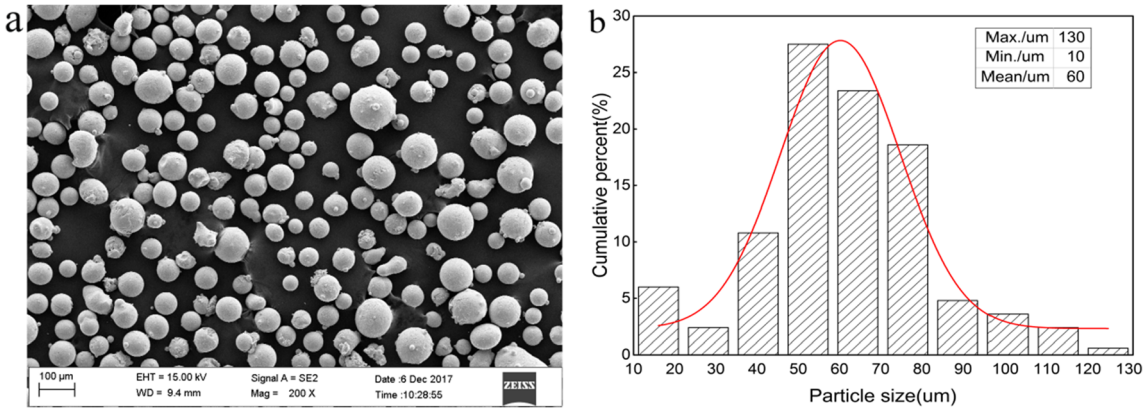

Fig. 1 SEM image showing **a** the 316L SS powder shape and **b** the particle size range

electrical discharge machining from each thin-wall sample in each substrate. Fig. 4 shows the dimensions schematic of HASP-produced tensile specimens according to GB/T228.1-2010. In addition, there were three samples tested per direction of each solution heat treatment and as-produced condition separately. Finally, the morphology of the tensile fracture surfaces was investigated by a super depth of field emission scanning electron microscope (SEM) at magnifications of 50× and 5000×. To study the homogeneity of solution heat treatment on the HASP-produced samples, Vickers micro-hardness measurements were executed by a 430SVD Vickers micro-hardness testing machine (made by Wilson Hardness, USA) on the polished surface with a load and loading time of 1000 gF and 10 s, respectively. At least 10 micro-hardness measurements were taken for each sample. Last but not least, the values of each micro-hardness point were calculated on the basis of the mean values of three indentations in the same region of three samples for each group.

2.4 Heat treatment of HASP-produced 316L specimens

The HASP-produced 316L specimens experienced different temperatures and times of solution heat treatment to study the evolution microstructure and mechanical properties.

1. Five groups of set 1 specimens to investigate the effect of the solution heat treatment temperature on the mechanical properties and microstructure. The first group was not heat treated and kept for comparison; those of other groups were solution heat treated at 950 °C, 1000 °C, 1050 °C and 1150 °C and underwent a 3-min heating duration; the next step was water quenching (WQ). The holding time of solution heat treatment of 316L stainless steel can be obtained according to the following empirical formula (1):

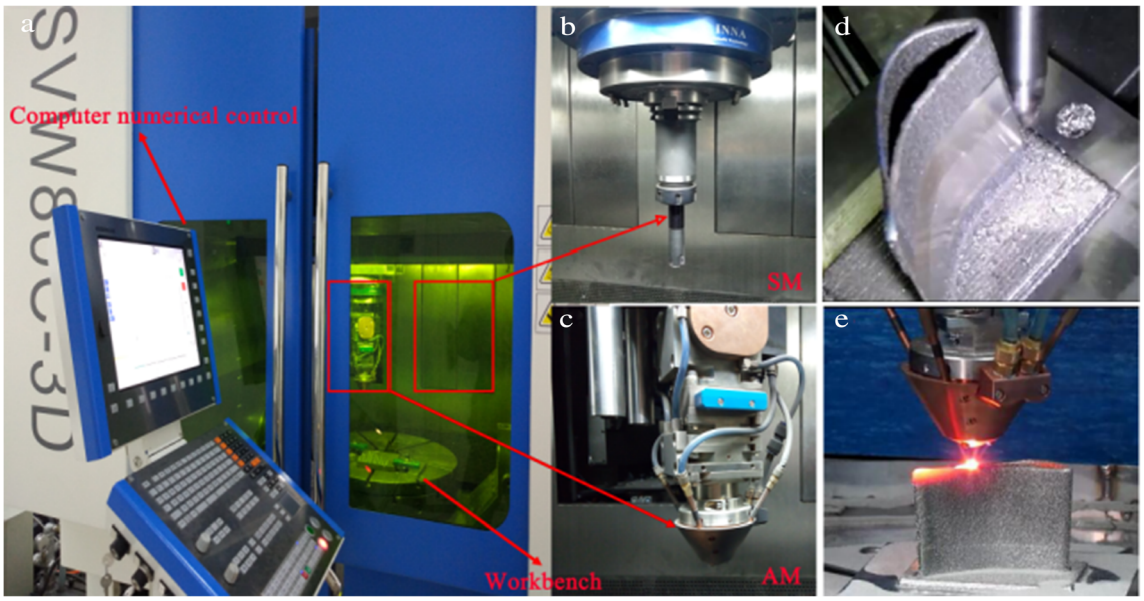

Fig. 2 **a** HASP machine (SVW80C-3D), with **b** CNC milling head, **c** DED head, **d** example of the CNC milling process, **e** example of the additive deposition process

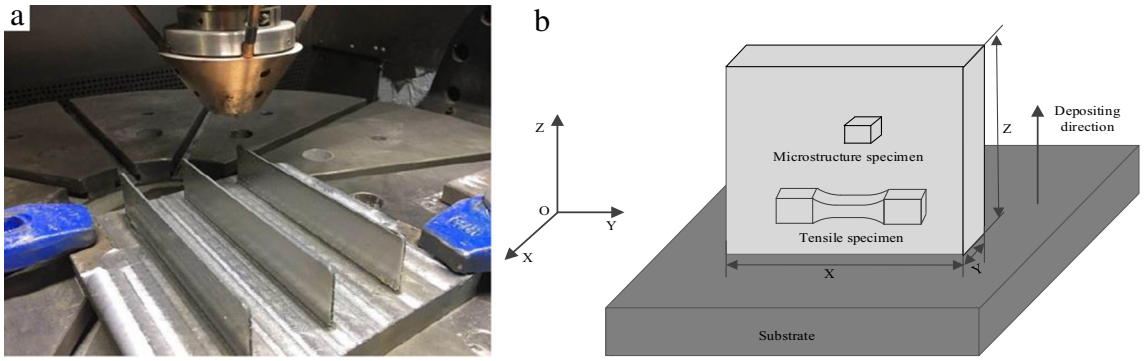

Fig. 3 HASP: **a** the final HASP-manufactured 316L samples and **b** the schematic illustration of the HASP-manufactured samples

$$T = 1.5 \cdot h \quad (1)$$

where T is the holding time (measured in minutes) of solution heat treatment and h is the thickness of the samples.

2. To study the influence of holding time of solution heat treatment on the mechanical properties, three groups of set 2 samples, including two groups, were solution heat treated for two different solution treatment holding times of 3 min and 30 min at 1150 °C, followed by WQ separately, and the other group was maintained in the as-manufactured state for comparison. Furthermore, heat treatment at 1150 °C for 30 min and then WQ were conducted to gain a completely austenitic microstructure.

3 Results and discussion

3.1 Microstructure features

The micrograph in Fig. 5 presents the effect of different solution heat treatment temperatures and dwell times on the microstructure in the same region of HASP-fabricated thin walls. And the heat treatment temperature vs time diagram and the samples' numbers are shown in Fig. 6 to better illustration the microstructure features. Fig. 5 a presents the microstructural image of the HASP before applying solution heat treatment parts, while Fig. 5 b–f show the influence of the solution heat treatment on the surface microstructures of the HASP 316L specimens. It is important to observe some variation in the content of both the σ and δ phase in the γ matrix of each microstructural constituent in the HASP-manufactured materials. In those micrographs, the lighter-etching stringers are σ phase, and the δ-ferrite is the dark-etching stringers. A proper heat treatment can be chosen to adjust the σ and δ phase content. An austenitic microstructure with a face centred cubic (FCC) structure can be acquired under a balanceable state on the basis of the chemical constituent of 316L stainless steel, and small amounts of less prevalent, finely dispersed δ-ferrite with a body centred cubic (BCC) structure were uniformly formed at the boundary of austenite grains owing to the existence of chemical elements (i.e. Mo, Cr and Si), and a rapid solidification rate can effectively promote the formation of the δ-ferrite. Moreover, there are no carbide precipitates in the austenitic steel as a result of a lower carbon content, which only makes up 0.02% of the 316L powder, as listed in Table 1 [24]. The HASP 316L samples before the heat treatment process have large amounts of strip morphology δ phase and the σ phase form in the strip, which results from high thermal gradients causing expansion owing to the rapid solidification rate in a very short time and the partial remelting of previously deposited layers followed by multiple thermal cycles occurring during each subsequent deposition in the DED process under the context of HASP, as shown in Fig. 5a.

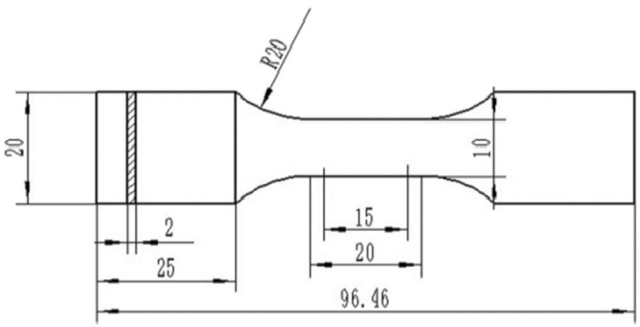

Fig. 4 Mechanical properties schematic: the dimensions of tensile samples

The response to heat treatment is a more uniform microstructure in most of the area of the heat-treated samples compared to the as-manufactured part. The strip structure is reduced until it becomes zero, suggesting that a complete microstructural transformation has occurred. As shown in Fig. 5 b and c, with the increase of temperature, an extremely fine-grained vermicular morphology of the σ and δ phases is displayed within the γ matrix. As shown in Fig. 5, when the temperature is 1050 °C for 3 min, the σ phase is replaced little by little within the γ matrix, but the δ phase with precious few alter of the primitive δ phase; however, the spheroidization

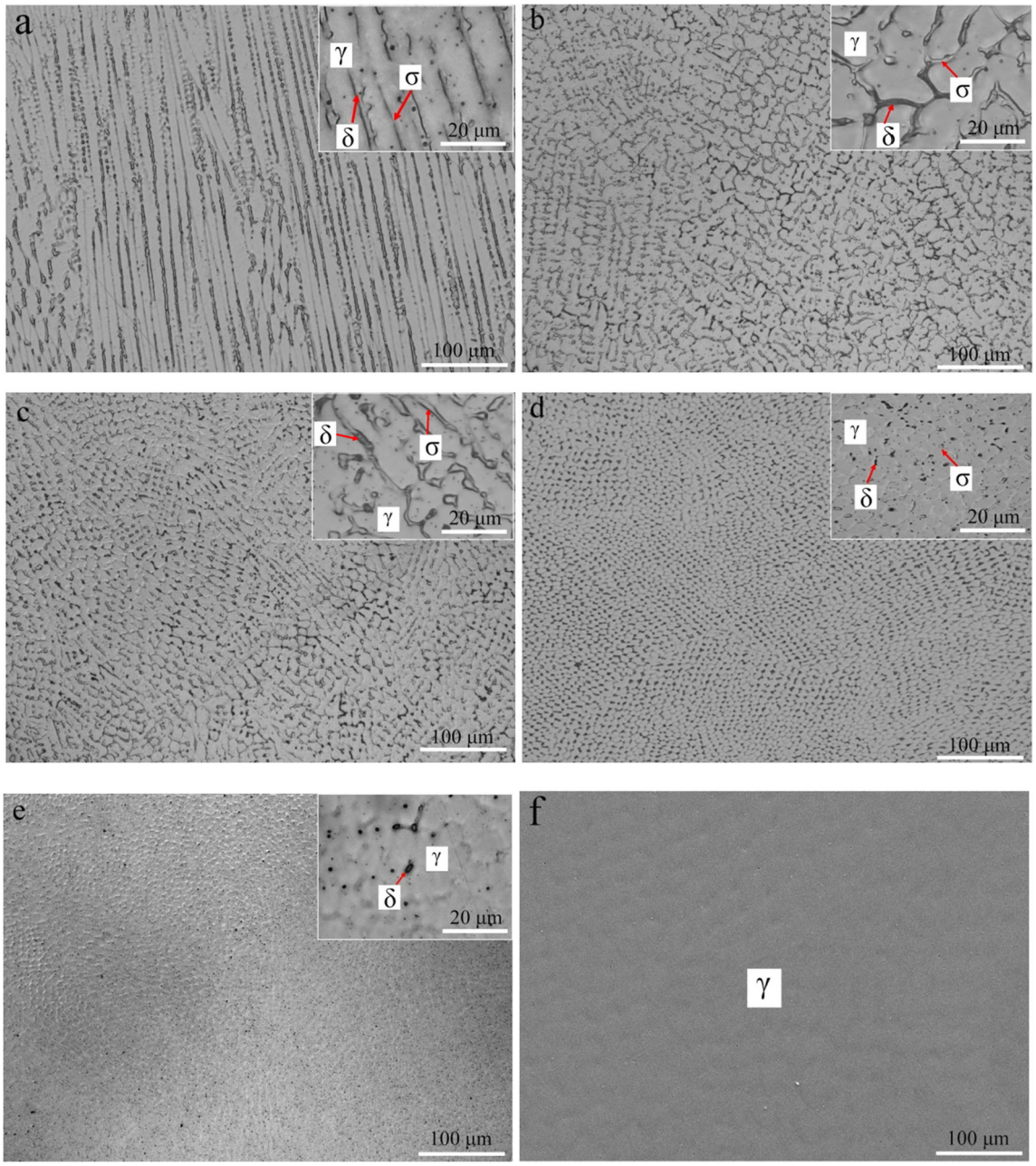

Fig. 5 Microstructures of HASP: **a** HASP without heat treatment; **b** 950 °C/3 min, WQ; **c** 1000 °C/3 min, WQ; **d** 1050 °C/3 min, WQ; **e** 1150 °C/3 min, WQ; **f** 1150 °C/30 min, WQ

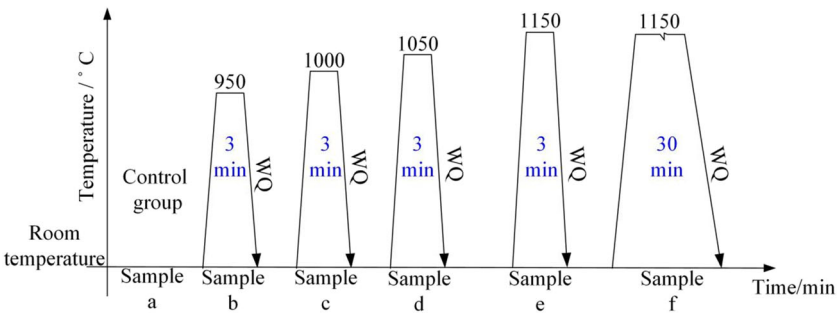

Fig. 6 Heat treatment process for HASP 316L samples: (a) HASP without heat treatment; (b) 950 °C/3 min, WQ; (c) 1000 °C/3 min, WQ; (d) 1050 °C/3 min; (e) 1150 °C/3 min, WQ; (f) 1150 °C/30 min, WQ.

treatment of all that remained of the δ phase and the amount of σ and δ phases decreases compared to that in Fig. 5 b and c. A dwell time of 3 min for the heat treatment temperature at 1150 °C led to the σ phase completely dissolving within the γ matrix and a portion of the δ phase within the γ matrix, and the particle morphology significantly decreased, as shown in Fig. 5e. With a heat treatment of 30 min or more at 1150 °C, there is a large difference in the phase content compared to the samples treated at 1150 °C for 3 min, which reduced the σ- and δ-phase content to virtually zero—indicating that the content of the σ and δ phases fully dissolved within the γ matrix progressively increased over time at that temperature until, after approximately 30 min, it transformed into the full austenitic microstructure, as shown in Fig. 5f. Therefore, as shown, changing the heat treatment temperature and dwell time can effectively change the content of the σ and δ phases. It can be observed that the fully austenitic microstructure is very widespread, thus verifying that the adopted solution heat treatment dramatically reduces the content of the δ-ferrite phase. Moreover, it is noted that the content of delta ferrite has a significant effect on the mechanical properties of materials [24]; a detailed discussion of this situation is presented in the next section.

3.2 Mechanical properties

Hardness is an indicator of great consequence for the material's capability to stand up to the plastic deformation. To assess the effect of the different solution heat treatment processes on the average micro-hardness of the HASP-fabricated 316L stainless steel samples, Vickers micro-hardness testing was carried out on the cross sections of the samples, and their corresponding experimental results for the average hardness values are depicted in Fig. 7. Generally, the average hardness values of the samples fabricated by HASP before applying solution heat treatment are higher than those after applying solution heat treatment because the σ and δ phases in the γ matrix can be seen visibly. The HASP-fabricated one before applying solution heat treatment has the maximum micro-hardness value, namely, 227 HV. Compared to the HASP-fabricated without heat treatment, the solution heat treatment temperature of 950 °C for 3 min resulted in a significant decrease of hardness. In addition, when further increasing the solution heat treatment temperature, the Vickers hardness decreased continuously. The average hardness of the HASP-fabricated 316L part underwent a continuous decrease from approximately 185 to 172 HV with the rise of the applied solution heat treatment temperature from 950 to 1000 °C in the same solution time for 3 min. Further raising the solution heat treatment temperature until the temperature reached 1050 °C, the Vickers hardness increased with an average value of approximately 179 HV because of the effect of hot working hardening, which caused the hardness to increase. When the solution temperature is higher than 1050 °C, up to 1150 °C, for 3 min, the Vickers hardness decreases a great deal. This is due to the increase of the solution heat treatment temperature, and the content of the σ and δ phases in the γ matrix can distinctly decrease, which causes the hardness to decrease. Furthermore, the hardness of the solution treatment time for 3 min is significantly higher than that for 30 min, which shows that the hardness of 316L SS decreases along with the rise of solution treatment time at the same temperature. The observed decrease in the hardness can be put down to the decrease of δ-phase content along with the increase of solution treatment time. A summarization all of the above phenomena can be explained as a superposition of these several types of strengthening and softening work together on the structure. As is known to all, the fully austenitic stainless steel parts demonstrate a greater possibility of hot-crack formation than those containing a small number of delta ferrite. It is found that there are still small amounts of delta ferrite, the austenite grain size growth is resisted, impurities are uniformly distributed and the total quantity of grain boundaries rises, which could delay crack formation. The existence of δ ferrite may arouse the hardness increase compared with the fully austenitic-single phase austenitic, as a result of the solid solution strengthening of the Mo and Ni of the ferritic phase [25]. Furthermore, the observed increase in the hardness can be put down to the generation of severe crystal lattice distortions because of small amounts of less-prevalent, finely dispersed δ-ferrite with BCC structure and austenitic microstructure with FCC structure; moreover, uniform distribution has larger obstacles to dislocation motion than the FCC structure. This explains why the existence of ferrite resulted in the fact that the hardness of the 316L SS was much higher than that of single-phase austenitic [25, 26].

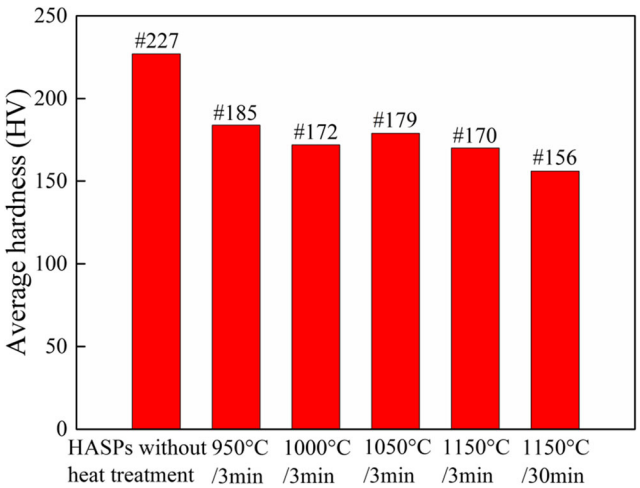

Fig. 7 Vickers hardness graphs for HASP 316L samples: (a) HASP without heat treatment; (b) 950 °C/3 min, WQ; (c) 1000 °C/3 min, WQ; (d) 1050 °C/3 min; (e) 1150 °C/3 min, WQ; (f) 1150 °C/30 min, WQ

The tensile stress-strain curves gained from the room temperature testing of 316L parts fabricated by HASP with different solution heat treatment processes were measured and contrasted with those of 316L specimens gained from HASP fabrication before applying solution heat treatment, as shown in Fig. 8, and the corresponding results are listed in Table 2. The tensile properties of HASP-fabricated 316L samples consist of ultimate tensile strength (UTS), yield strength (YS) and elongation to failure (ETF), and their comparison with traditional 316L by casting [22, 23] are listed in Table 2. The results demonstrate that the HASP before applying solution heat treatment sample displays the maximum UTS and YS of 596.6 MPa and 421.1 MPa, respectively, but has the lowest ETF of 43.3%. The solution heat treatment has a considerable effect on the mechanical properties of the HASP-produced 316L sample. The results showed that the UTS and YS show a declining trend. Meanwhile, the ETF was increased along with the increase of the solution temperature. When the specimen undergoes solution heat treatment at 950 °C for 3 min, there is a rather significant reduction in both UTS and YS (560.2 MPa and 378.7 MPa, respectively), while there is a great improvement in ETF of 49.7 % compared to the HASP-fabricated one before applying solution heat treatment. The heat treatment temperature rises from 950 to 1000 °C, the UTS and YS decrease from 560.2 and 378.7 to 535.5 and 337.8 MPa, respectively, while the ETF increases from 49.7 to 51.2%. By continuing to raise the solution heat treatment temperature to 1050 °C for 3 min, the UTS is decreased to 530.1 MPa, while the ETF and YS increase to 52.8% and 353.6 MPa, respectively. However, when the solution temperature reaches 1150 °C for 3 min, the results show that the UTS and YS decrease further (509.5 MPa and 308.1 MPa, respectively), while the ETF marginally increases to a higher value of 54.6% in comparison with the other solution temperature. For the specimens that go through the same solution heat treatment temperature, the UTS and YS are steadily reduced from 509.5 to 497.3 MPa and from 308.1 to 242.5 MPa, respectively, and the ETF increases to the maximum, which is from 54.6 up to 62.4%, indicating superior ductility, as the solution holding time increases from 3 to 30 min. In addition, another conclusion that can be drawn from Table 2 is that the tensile strength of the specimen fabricated by HASP with solution heat treatment temperature at 1150 °C for 30 min is slightly lower than that of traditional 316L by casting material. Moreover, the ETF is 13.45% higher than that of traditional 316L by casting, showing a superior ductility.

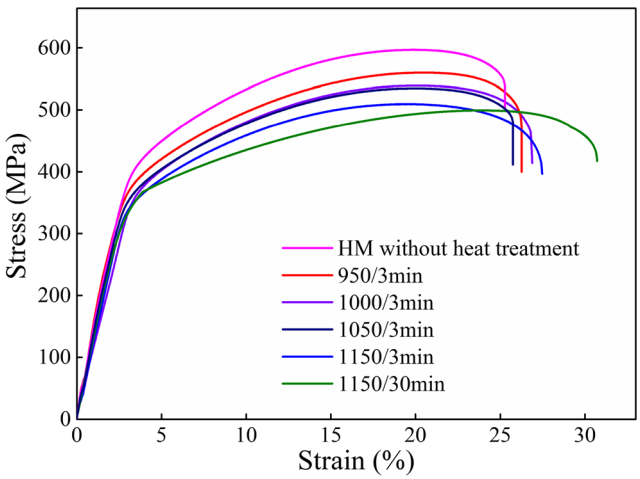

Fig. 8 Stress/strain curves of the HASP before and after being solution heat treatment 316L tensile specimens

Table 2 Room-temperature tensile properties of the HASP before and after solution heat treatment of the 316L tensile specimens as well as comparison with casting

	UTS/MPa	YS/MPa	ETF/%
HASP without heat treatment	596.6	421.1	43.3
950 °C/3 min, WQ	560.2	378.7	49.7
1000 °C/3 min, WQ	535.5	337.8	51.2
1050 °C/3 min, WQ	530.1	353.6	52.8
1150 °C/3 min, WQ	509.5	308.1	54.6
1150 °C/30 min, WQ	497.3	242.5	62.4
casting	552	262	55

The UTS and YS, as well as ETF, after solution heat treatment are affected by a couple of factors consisting of the number, size and morphology of the grain, content of the δ phase, initial hardening rate and recovery rate. As to the strength of the HASP-fabricated 316L specimen before and after applying solution heat treatment samples in this study, three sections are to be addressed. First, by increasing the solution heat treatment temperature and time to approximately 30 min, the content of the δ phase gradually decreases until finally disappearing, which transforms into the full austenitic microstructure. Small amounts of δ-ferrite with BCC structure before applying solution heat treatment samples change to austenitic microstructure with FCC structure after applying heat treatment one. The dislocation motion must overcome greater resistance of BCC lattice than that of FCC lattice, which means the BCC structure with the higher yield strength. The higher misorientation angle results in a higher dislocation density in heat treatment samples, which may also be useful in making the higher strain hardening rate. Second, the high strength of the HASP-fabricated 316L samples can be connected with the small grain size. Grain size had some impact on the mechanical properties to achieve the rationalization by the semi-empirical Hall-Petch (HP) formula [27, 28]. In general, solution heat treatment of the 316L samples was found to increase the grain size and the angle boundaries, and this is a significant reason that reduces the yield strength of the heat treatment samples. Third, the solution heat treatment decreases the residual stresses that come into being under the

DED process during the HASP. Based on the above three points, in favour of the improvement of the ductility of the solution heat treatment 316L samples, this explains why the existence of ferrite leads to the fact that the strength was much higher than that of the single-phase austenitic stainless steel.

The tensile fracture of the 316L stainless steel is intersected with the principal stress at an angle of 45°, the fracture surface has a fibrous shape and the colour is dark. That is consistent with the macroscopic appearance of a ductile fracture, which is obviously a ductile fracture. Fig. 9 shows the SEM from the tensile fracture surfaces of the 316L samples before and after applying the solution heat treatment (1050 °C/3 min), respectively. The heat treatment (1050 °C/3 min) sample after applying the solution heat treatment has an even greater reduction in area than the HASP-fabricated sample before the solution heat treatment, as shown in Fig. 9 a and b. A large number of classic dimple structures were observed in the high magnification of the morphologies on the tensile fracture surfaces in Fig. 9 c and d, which are indicative that the fracture behaviour of HASP-fabricated samples without heat treatment and after applying solution heat treatment to the 316L samples belongs to ductile fracture characteristics. Compared with Fig. 6 c and d, the HASP-fabricated sample before applying the solution heat treatment has a small dimple size and inhomogeneous distribution of the dimples, while the solution heat treated one is uniform, the dimples are relatively rare and the size is relatively large. The fracture morphology analysis shows that there are a number of deep dimples of large size in the microstructure of the heat treatment sample, which proved that the resistance of crack propagation is comparatively large. Therefore, the toughness is better than that of the sample without the solution heat treatment. In addition, unmelted powder particles could be seen along the fracture surface of the heat treatment HASP-fabricated specimen in Fig. 9d, which may come down to the lack of fusion in the DED process under the context of HASP. This shows that unmelted powders are, up to a point, not affected by the homogenizing heat treatment selected.

4 Conclusions

The effects of the solution heat treatment on the microstructural characterization and the resulting mechanical properties of AISI 316L SS specimens produced by using hybrid additive and subtractive processes (HASP) have been studied. The following main conclusions and findings can be obtained from this study:

1. When the heat treatment is less than 1050 °C, different amounts of the σ and δ phases exist in the γ matrix, and with the rise of the solution heat treatment temperature, the content of the σ phase and the spheroidization of the remaining δ phase progressively decrease. The δ phase decreases and the σ phase completely dissolves as the heat treatment temperature increases up to 1150 °C for 3 min. Prolonging the holding time at 1150 °C to 30 min leads to grain coarsening, with the δ and σ phases fully dissolved into the γ matrix.
2. The decrease of the σ and δ phases causes the decrease of the ultimate tensile strength (UTS) and yield strength (YS) but the increase of the elongation to failure (ETF) of 316L samples. The tensile properties of HASP before

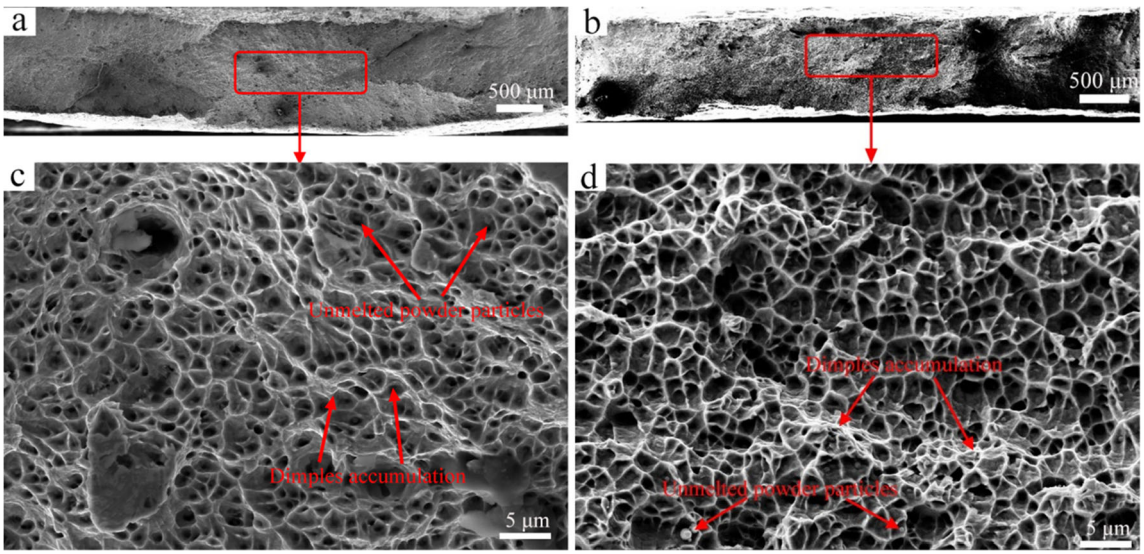

Fig. 9 Tensile fracture surfaces of HASP samples in **a** HASP before applying solution heat treatment and **b** after being solution heat treatment conditions. Higher magnification of dimples on fracture surfaces of **c** HASP before applying solution heat treatment and **d** after applying solution heat treatment samples

and after applying solution heat treatment to the 316L samples all exceed industrial demand. With the solution temperature and time increases, the size of the grain raises, but their number decreases, which will lead to lower the Vickers hardness. Compared with HASP before applying solution heat treatment to the specimens, more ductility was exhibited for HASP after applying heat treatment to the samples.

3. The best solution treatment for 316L SS specimens with a thickness of 2 mm is as follows: set the temperature to 1050 °C for 3 min and then water quench (WQ). The internal structure of the sample is uniform; the mechanical properties are obviously improved, including the hardness, which increases to 179 HV; the tensile strength and yield strength are 530.1 MPa and 353.6 MPa, respectively; and the elongation to failure is as high as 52.8%.
4. These findings could provide the foundation for optimizing the solution heat treatment to fabricate 316L components using HASP processing technologies to achieve materials with specific microstructure and mechanical properties for all sorts of applications.

Acknowledgements The authors sincerely thank Mr. Y.D. Gong, for their critical discussion and reading during manuscript preparation.

Code availability Not applicable.

Author contribution Shuoshuo Qu: investigation, methodology, experiment, writing—original draft, experiment. Yadong Gong: conceptualization, funding acquisition, reviewed and edited the manuscript, supervision. All authors read and approved the final manuscript.

Funding This research has been supported by the National Natural Science Foundation of China under Grant No.51775100 and No.51875321, and the Fundamental Research Funds for the Central Universities under Grant No.N180306001.

Declaration

Ethics approval The authors state that the present work is in compliance with the ethical standards.

Consent to participate Not applicable.

Consent to publish All authors agree to publish.

Competing interests The authors declare no competing interests.

References

1. Gray GT, Livescu V, Rigg PA, Trujillo CP, Cady CM, Chen SR, Carpenter JS, Lienert TJ, Fensin SJ (2017) Structure/property (constitutive and spallation response) of additively manufactured 316L stainless steel. Acta Mater 138:140–149
2. AlMangour B, Grzesiak D, Borkar T, Yang JM (2018) Densification behavior, microstructural evolution, and mechanical properties of TiC/316L stainless steel nanocomposites fabricated by selective laser melting. Mater Des 138:119–128
3. Campanelli SL, Angelastro A, Signorile CG, Casalino G (2017) Investigation on direct laser powder deposition of 18 Ni (300) marage steel using mathematical model and experimental characterization. Int J Adv Manuf Technol 89(1-4):885–895
4. Khorasani AM, Gibson I, Asadnia M, O'Neill W (2018) Mass transfer and flow in additive manufacturing of a spherical component. Int J Adv Manuf Technol 96(9-12):3711–3718
5. Zhu LD, Xu PS, Lan Q, Meng GR, Ren Y, Yang ZC, Xu PH, Liu Z (2019) Recent research and development status of laser cladding: a review. Opt Laser Technol 138:106915
6. AlMangour B, Baek MS, Grzesiak D, Lee KA (2018) Strengthening of stainless steel by titanium carbide addition and grain refinement during selective laser melting. Mater Sci Eng A 712:812–818
7. Li S, Wei QS, Shi YS, Chua CK, Zhu ZC, Zhang DQ (2015) Microstructure characteristics of Inconel 625 superalloy manufactured by selective laser melting. J Mater Sci Technol 31 (9):946–952
8. Zhu Z, Dhokia V, Newman ST, Nassehi A (2014) Application of a hybrid process for high precision manufacture of difficult to machine prismatic parts. Int J Adv Manuf Technol 74(5-8):1115–1132
9. Yadollahi A, Shamsaei N, Thompson SM, Seely DW (2015) Effects of process time interval and heat treatment on the mechanical and microstructural properties of direct laser deposited 316L stainless steel. Mater Sci Eng A 644:171–183
10. Zhu ZC, Dhokia V, Nassehi A, Newman ST (2016) Investigation of part distortions as a result of hybrid manufacturing. Robot Comput Integr Manuf 37:23–32
11. Liu JK, To AC (2017) Topology optimization for hybrid additive-subtractive manufacturing. Struct Multidiscipl Optim 55(4):1281–1299
12. Kianersi D, Mostafaei A, Amadeh AA (2014) Resistance spot welding joints of AISI 316L austenitic stainless steel sheets: phase transformations, mechanical properties and microstructure characterizations. Mater Des 61:251–263
13. Lippold JC, Savage VF (1979) Solidification of austenitic stainless steel weldments: part I-a proposed mechanism. Weld J 58:362–374
14. Ben Rhouma A, Amadou T, Sidhom H, Braham C (2017) Correlation between microstructure and intergranular corrosion behavior of low delta-ferrite content AISI 316L aged in the range 550-700 degrees C. J Alloys Compd 708:871–886
15. Wang CC, Tan XP, Liu EJ, Tor SB (2018) Process parameter optimization and mechanical properties for additively manufactured stainless steel 316L parts by selective electron beam melting. Mater Des 147:157–166
16. Lo KH, Shek CH, Lai JKL (2009) Recent developments in stainless steels. Mater Sci Eng R Rep 65(4-6):39–104
17. Olabi AG, Hashmi MSJ (1995) The effect of post-weld heat-treatment on mechanical-properties and residual-stresses mapping in welded structural steel. J Mater Process Technol 55(2):117–122
18. Zhu HH, Fuh JYH, Lu L (2007) The influence of powder apparent density on the density in direct laser-sintered metallic parts. Int J Mach Tools Manuf 47(2):294–298
19. Yadroitsev I, Krakhmalev P, Yadroitsava I (2015) Hierarchical design principles of selective laser melting for high quality metallic objects. Addit Manuf 7:45–56
20. Yang YY, Gong YD, Qu SS, Rong YL, Sun Y, Cai M (2018) Densification, surface morphology, microstructure and mechanical properties of 316L fabricated by hybrid manufacturing. Int J Adv Manuf Technol 97(5-8):2687–2696
21. Karunakaran KP, Suryakumar S, Pushpa V, Akula S (2010) Low cost integration of additive and subtractive processes for hybrid

layered manufacturing. Robot Comput Integr Manuf 26(5):490–499
22. Yang YY, Gong YD, Li CH, Wen XL, Sun JY (2021) Mechanical performance of 316 L stainless steel by hybrid directed energy deposition and thermal milling process. J Mater Process Technol 291:117023
23. Yang YY, Gong YD, Qu SS, Xie HL, Cai M, Xu YC (2020) Densification, mechanical behaviors, and machining characteristics of 316L stainless steel in hybrid additive/subtractive manufacturing. Int J Adv Manuf Technol 107(1-2):177–189
24. Chen XH, Li J, Cheng X, He B, Wang HM, Huang Z (2017) Microstructure and mechanical properties of the austenitic stainless steel 316L fabricated by gas metal arc additive manufacturing. Mater Sci Eng A 703:567–577
25. Zhang K, Wang S, Liu W, Shang X (2014) Characterization of stainless steel parts by laser metal deposition shaping. Mater Des 55:104–119
26. Kocijan A, Merl DK, Jenko M (2011) The corrosion behaviour of austenitic and duplex stainless steels in artificial saliva with the addition of fluoride. Corros Sci 53:776–783
27. Basariya MR, Srivastava VC, Mukhopadhyay NK (2014) Microstructural characteristics and mechanical properties of carbon nanotube reinforced aluminum alloy composites produced by ball milling. Mater Des 64:542–549
28. Dong XH, Hong XT, Chen F, Sang BR, Yu W, Zhang XP (2014) Effects of specimen and grain sizes on compression strength of annealed wrought copper alloy at room temperature. Mater Des 64:400–406